Applied Surface Science 280 (2013) 343–348

Contents lists available at SciVerse ScienceDirect

Applied Surface Science

journal homepage: www.elsevier.com/locate/apsusc

Surface and interference co-enhanced Raman scattering from indium tin oxide nanocap arrays

Yimin Yang[a,*], Teng Qiu[a,b,**], Zhichang Liu[a], Qi Hao[a], Xianzhong Lang[a,b], Qingyu Xu[a], Gaoshan Huang[c], Paul K. Chu[b]

[a] Department of Physics and Key Laboratory of MEMS of the Ministry of Education, Southeast University, Nanjing 211189, People's Republic of China
[b] Department of Physics and Materials Science, City University of Hong Kong, Tat Chee Avenue, Kowloon, Hong Kong, People's Republic of China
[c] Department of Materials Science, Fudan University, Shanghai 200433, People's Republic of China

ARTICLE INFO

Article history:
Received 15 March 2013
Received in revised form 24 April 2013
Accepted 25 April 2013
Available online 16 May 2013

Keywords:
Indium tin oxide
Surface-enhanced Raman scattering
Porous anodic alumina

ABSTRACT

Large-area indium tin oxide (ITO) nanocap arrays are fabricated on porous anodic alumina (PAA) templates to produce robust and cost-effective surface-enhanced Raman scattering (SERS) substrates. The electromagnetic enhancement mechanism is believed to be the main reason for the enhancement. The topography of the ITO nanocap arrays can be adjusted to optimize the enhancement factor by varying the anode voltage applied to the PAA templates. The optical interference in enhanced Raman scattering from the ITO nanocap arrays with different thicknesses are systematically studied and optical self-interference from the incident, scattered, and emitted light is observed to modulate the intensity and shape of the Raman signals.

1. Introduction

Indium tin oxide (ITO) is one of the most widely used transparent conducting oxides because of its electrical conductivity and optical transparency and it can be deposited as a thin film. Recently, experimental observation of the surface plasmon resonance (SPR) effects from ITO has implications to solid state and surface science as well as optical applications to sensing and analysis [1–3]. It has been reported that SPR from ITO is similar to that observed from noble metals and free from interferences from interband transitions [4]. Compared to noble-metal nanostructures, ITO has the following additional advantages. First of all, ITO has no inter- and intra-band transitions in the vis-NIR region permitting systematic studies of the origin of the optical effects arising from SPR of conduction electrons [4]. Secondly, ITO can have a range of compositions resulting from different metal doping and oxygen content. The SPR frequency can thus be tuned by changing the thin film preparation technique or changing the In/Sn molar ratio [3]. Thirdly, ITO is often used to make transparent conductive coatings in displays. SPR thus has a positive impact on the performance of integrated optical devices such as organic light-emitting diodes and solar cells that make use of ITO as a transparent electrode [5]. Fourthly, ITO is chemically and thermally stable. No protective layers are needed in long-time measurements to monitor biological interactions [2].

One of the attractive aspects of SPR is that subwavelength structures can be used to concentrate and channel light and produce electric field enhancement that can be utilized to manipulate light–matter interactions and boost non-linear phenomena [6]. In particular, the enhanced localized electromagnetic (EM) field near the nanostructured surface gives rise to surface-enhanced Raman scattering (SERS) [7]. SERS has been observed from embedded ITO prepared by pulsed laser deposition of ITO films on Si templates with a roughened surface [8] and recent work by Zhao et al. shows that the Raman enhancement from ITO nanorods is comparable to that observed from Au nanorods [9]. Nevertheless, fabrication of ITO nanostructures with evenly distributed plasmonic fields and reliable SPR properties is still challenging and more research is needed to spur wider use of ITO in chemical and biological sensing. In this work, periodically patterned ITO nanocap arrays are fabricated on porous anodic alumina (PAA) templates to produce robust and cost-effective SERS substrates with significant Raman enhancement. The use of PAA templates to fabricate SERS-active substrates is promising considering the easy fabrication, excellent reproducibility, modest cost, and large area production [10]. Moreover, this technique can create long-range uniform plasmonic structures up to the cm dimensions [11]. Because of the optical transparency, the influence of the interference phenomenon in ITO nanocap arrays is investigated and our results demonstrate that the interference effect is substantial.

* Corresponding author. Tel.: +86 25 52090600.
** Co-corresponding author.
E-mail addresses: yangyimin@seu.edu.cn, 101010713@seu.edu.cn (Y. Yang), tqiu@seu.edu.cn (T. Qiu).

0169-4332/$ – see front matter © 2013 Elsevier B.V. All rights reserved.
http://dx.doi.org/10.1016/j.apsusc.2013.04.158

2. Experimental details

High-purity aluminum (Al) foils (99.99%) were degreased by acetone and then electropolished using a mixture of ethanol and perchloric acid with a volume ratio of 5:1 at a constant DC voltage of 15 V for 3 min to further remove surface impurities. After rinsing in distilled water and drying, the Al foils were anodized separately in a 0.3 M oxalic acid solution at a DC voltage of 30 V, 40 V, 50 V, or 60 V at 5 °C. In order to obtain an ordered nanopore array, a two-step anodizing process was adopted. The Al foils were first anodized for 2 h (30 V, 40 V, and 50 V) and 30 min (60 V) followed by immersion in a mixture of chromic acid (1.8 wt.%) and phosphoric acid (6 wt.%) at 75 °C (1:1 in volume). The anodization time in the second step was 15 min (30 V), 6.5 min (40 V), 2 min (50 V) and 40 s (60 V), respectively and the PAA templates were obtained.

The ITO nanocap arrays were prepared on the PAA templates by pulsed laser ablation (248 nm KrF laser, 300 mJ/pulse, 3.0 Pa oxygen, 10 Hz) of an ITO target (In_2O_3 92 wt.%, SnO_2 8 wt.%) at room temperature. Uniform ITO films were deposited by rotating the PAA substrates during ITO deposition. Thickness-continue ITO films were deposited by immobilizing the PAA substrates during ITO deposition. Similar films were deposited on Si substrates to determine the film thickness or thickness-distribution more accurately. To improve crystallization and conductivity, the samples were annealed at 500 °C in vacuum (2×10^{-4} Pa) for 30 min.

Scanning electron microscopy (SEM, JEOL JSM-6335F) and atomic force microscopy (AFM, Vecco MultiMode V) were used to investigate the structures of ITO nanocap arrays. The Raman measurements were performed on a Jobin Yvon LabRAM HR800 micro-Raman spectrometer with the 514 nm laser line at room temperature. An area of ~2 μm in diameter was probed by a 50× objective lens (nominal aperture 0.45) and the incident power at the sample was 0.2 mW. The signal acquisition time was 10 s. To evaluate the Raman enhancing capability of the materials, a Rhodamine 6G (R6G) water solution was used. 8 μL of the R6G solution was added to the substrate and after the water was vaporized, a circular mark with a diameter of 3 mm remained on the substrate. The acquisition time and laser power were the same for all Raman spectra. The SERS spectra were recorded from multiple sites on the substrate to improve and confirm reproducibility. Similar SERS spectral characteristics such as enhancement, position, and relative intensity of the bands were determined from various locations to confirm large-area and uniform production.

3. Results and discussion

The use of the PAA templates in conjunction of the versatile coating technique allows flexible and rapid production of the nanocap arrays [10]. With the exception of the ordered hexagonal pore arrays on the PAA templates, there are small protrusions along the surface of the pore wall, and a dent exists between two neighboring protrusions. The open features of the pores caused by volume expansion when aluminum is converted into alumina can be used as templates to design and fabricate the nanostructured platform in which the areas exhibiting large gap-related enhancement are organized in a regular pattern. Fig. 1 shows a representative cross-sectional SEM image of the ITO nanocap array on the PAA template. The thickness of the ITO layer is 22 nm and that of PAA layer is 380 nm. Protrusions can be observed along the surface of the pore wall. There is a V-shape dent between two adjacent protrusions (see the inset) and the hot spots are believed to be located in these V-shape ortho-cap gaps. The ITO nanocaps separated by tunable gaps can be fabricated on the PAA templates with different nanopore diameters, which can be controlled by adjusting the anode voltage. Fig. 2 depicts a series of 3D AFM images of the ITO nanocap arrays

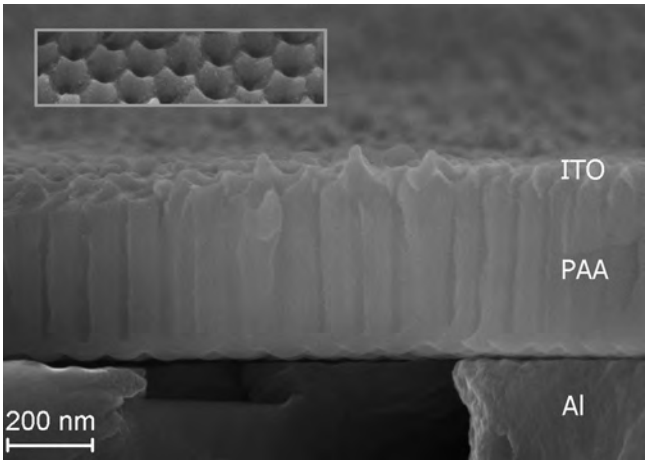

Fig. 1. Representative cross-sectional SEM image of the ITO nanocap array. The inset is a surface image at a 30° tilt.

formed at different anodic voltages. The thickness of the ITO layer is 22 nm. As shown in the AFM images in Fig. 2, these ITO nanocaps cover the alumina protrusions and exhibit a periodic hexagonal arrangement. It can be observed that perfect self-organized growth, which controls the nanopore arrangement, only occurs at a certain anodic voltage of 40 V. The detailed structural parameters of ITO nanocap arrays are shown in Table 1 and in general, a high SERS activity results from a high density of hot spots, high order, and large surface roughness.

To evaluate the Raman-enhancing capability of the ITO nanocap arrays, an R6G solution (3.3×10^{-6} M) is applied to the ITO/PAA/Al substrates. Fig. 3A shows a series of spectra illustrating the efficiency of SERS. Many salient Raman peaks can be observed from the R6G probe. The Raman intensity varies substantially with different nanopore diameters. The Raman enhancement observed from the ITO/PAA(40 or 50 V)/Al substrates is evident larger than from ITO/PAA(30 or 60 V)/Al substrates. The difference in spectral shape between the 40 and 50 V samples is result of different influence by interference effect which will be discussed later. The strong enhancement can be attributed to that the nanocap arrays are assembled with a favorable gap configuration and highly ordered

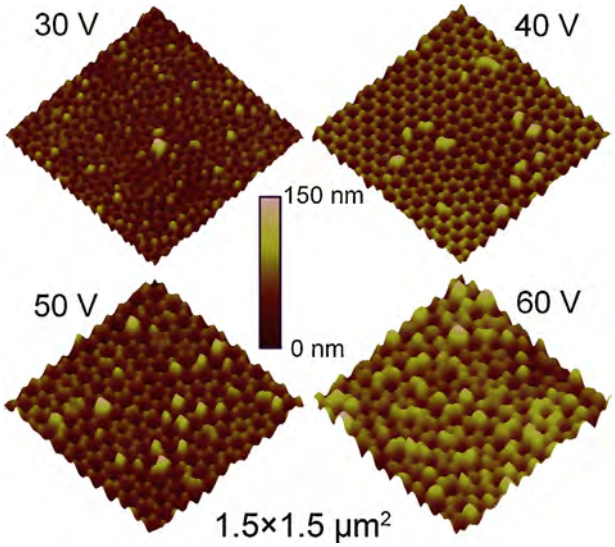

Fig. 2. 3D AFM image (1.5×1.5 μm^2) acquired from the ITO coated PAA membranes formed under different constant DC voltages: 30, 40, 50 and 60 V. The thicknesses of the ITO layer are all set to be 22 nm.

Table 1
Structural parameters of ITO nanocap arrays shown in Fig. 2.

DC voltage (V)	30	40	50	60
Para-cap spacing (nm)	70	104	134	153
Pore diameter (nm)	22	33	40	48
Pore density (cm^{-2})	3.14×10^{10}	1.42×10^{10}	0.85×10^{10}	0.65×10^{10}
Surface roughness (nm)	9.4	13.1	16.0	21.8

arrangement. Together with a high density of both ITO nanocaps and hot spots, intense SERS enhancement can be achieved. In comparison, R6G adsorbed directly on a quartz substrate exhibits no visible R6G Raman bands but only a strong fluorescence background. The fact that the fluorescence from the R6G molecular probes is largely quenched on the ITO surface suggests that the excited electrons from the R6G molecules transfer with an ultrafast and nonradiative decay rate into the dissipative modes of the ITO layer. This is expected from molecules adsorbing directly on metallic surfaces and in agreement with electromagnetic prediction [12].

Fig. 3B shows the intensity of the SERS signal at 612 cm^{-1} as a function of molar concentration on a logarithmic scale. A linear behavior appears from 1×10^{-7} to 1×10^{-5} M with a proportionality constant of unity, suggesting that the number of adsorption sites with high Raman enhancement is large enough to accommodate a considerable range of sample concentrations. When the concentration is increased to more than 1×10^{-5} M, a strong fluorescence background emerges, indicating that adsorption of R6G onto sites with high enhancement becomes saturated as multilayers of R6G molecules begin to accumulate on the surface. Low detection of R6G probes of 1×10^{-7} M or 50 ng/mL is observed here and it is much lower than the reported 1–10 μg/mL on ITO nanorods [9]. Considering that silver has a highest quality factor (Ag 392, Au 16.66, ITO 2.72), the typical silver nanocap array is chosen as a reference in this study. A silver film with a thickness of 22 nm is evaporated onto a PAA membrane (40 V) at room temperature. Similar SERS spectral characteristics [see the top of Fig. 3A] such as the position and relative intensity of the bands are determined from the silver nanocap array. With regard to the silver nanocap arrays, the intensities of the Raman signal at 612 cm^{-1} at two R6G concentrations are shown in Fig. 3B which discloses that the enhancement capability of the ITO/PAA/Al substrate is 3.9% of that of the Ag/PAA/Al substrate. Here, the enhancement capability of ITO nanocap arrays is comparing with that of new-prepared silver structure. However, due to chemical instability, the formation of silver oxidation or a protecting layer will cause the enhancement capability of silver structure evidently degrade. This is because the light field of surface plasmons exponentially decays from the metal surface, as a result, the molecular probes have to be near the metal surface in SERS experiments. In contrary, after several months, the Raman activity of the ITO structure is essentially unchanged.

The homogeneity of the ITO nanocap arrays is evaluated by 2D point-by-point SERS mapping of the R6G molecules. Fig. 3C shows a typical SERS map of the ITO nanocap array. Excellent uniformity over a large area of 40.0 μm × 40.0 μm is achieved by measuring 400 points at a regular step of 2 μm. The relative SERS peak intensity of the collection spots is centered in a narrow range and the spot-to-spot relative standard deviation is 7%. This suggests that the substrate homogeneity is quite good and strict control of

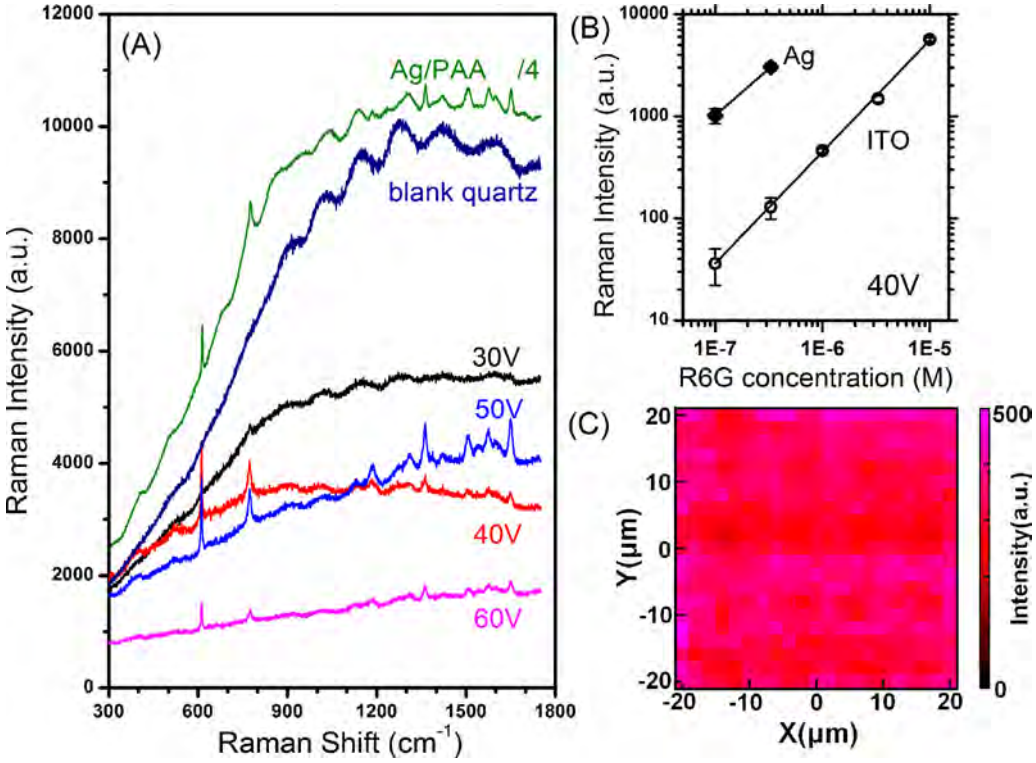

Fig. 3. (A) SERS spectral comparison of 3.3×10^{-6} M R6G adsorbed on the ITO coated PAA membranes formed under different constant DC voltages (samples in Fig. 2) and a blank quartz substrate and 3.3×10^{-7} M R6G adsorbed on silver coated PAA membrane formed under 40 V. (B) SERS signal at 612 cm^{-1} as a function of the R6G molecular concentration on a logarithmic scale: ITO/PAA(40 V)/Al substrate (open circles) and Ag/PAA(40 V)/Al substrate (solid diamonds). Solid line is a guide to the eye. (C) Typical SERS map (40 μm × 40 μm) obtained from the ITO nanocap array (40 V).

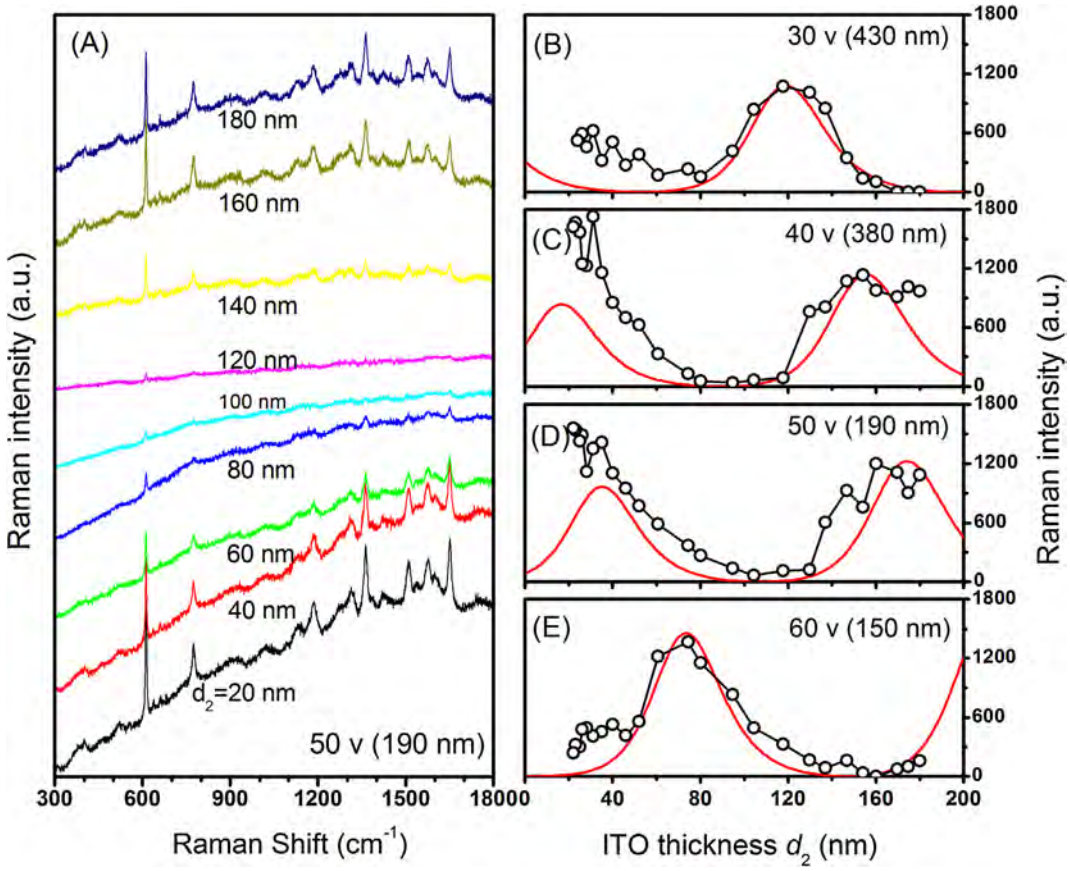

Fig. 4. (A) Variation of SERS spectra of R6G molecular probes with the increasing of thickness of ITO films on PAA (50 V) membrane. (B)–(E) SERS intensities of the Raman signal at 612 cm^{-1} as a function of the ITO thickness, the PAA membranes were anodized at (B) 30 V, (C) 40 V, (D) 50 V and (E) 60 V. Open circles are the experimental data. Solid lines are the theoretical intensity distributions calculated using interference factor $F(d_2, d_3, \lambda_1, \lambda_2)$. In calculations, parameters were set as $\lambda_1 = 514.5$ nm, $\lambda_2 = 531$ nm and $a = 3$.

the preparation conditions can ensure good reproducibility among different batches.

Because of the optical transparency of both ITO nanostructure and PAA membrane, the influence of interference phenomenon on the enhanced Raman signals is also investigated. Fig. 4A shows the enhanced Raman spectra acquired from the 3.3×10^{-6} M R6G probe on 20–180 nm ITO on a PAA (50 V) membrane. The Raman signals and fluorescence background are strongly affected by the thickness of the ITO film showing variations of up to 24 times in the Raman signals. The detailed variations are shown as a function of ITO film thickness [intensity at 612 cm^{-1} is used] with different nanopore diameters in Figs. 4B–E. The position of the peaks depends on the PAA membrane thickness. It is noted that the fluctuations in the Raman signals with film thickness follow the color variation in the reflective interference fringes [see Fig. S1], which is caused by optical interference between the surface and interface of a transparent film [13].

The interference effect on SERS of ITO/Si(etched) substrate is discussed in the context of a multi-reflection model [13,14]. Fig. 5A shows the schematic diagram of the optical self-interference in the air/ITO/PAA/Al structure. Multiple reflections occur in the transparent ITO layer and the PAA membrane. Three self-interference sources including the incident light, scattered light, and emitted light are considered separately. The three sources determine the spectral intensity and shape. In the air (phase 1)/ITO (phase 2)/PAA (phase 3)/Al (phase 4) system, the combined modification factor of the interference effects can be written as $F(d_2, d_3, \lambda_1, \lambda_2) = f_1(d_2, d_3, \lambda_1) \cdot f_2(d_2, d_3, \lambda_2)$, where $f_1(d_2, d_3, \lambda_1)$ refers to the change in light absorption due to self-interference of the incident light at wavelength λ_1 and $f_2(d_2, d_3, \lambda_2)$ is the change in the detected intensity due to self-interference of the scattered or emitted light at wavelength λ_2.

Considering that the backscattering configuration is adopted and that the size of the porous structure is much smaller than the wavelength of the incident light, the theoretical treatment on the reflection from a surface of a porous material is simplified to the reflection from a flat surface where the effective refractive index of the porous material is needed. Such a simplification has been adopted to study optical oscillation in PAA layer by Huang et al. [15] and Gardelis et al. [16]. Finally,

$$f_1(d_2, d_3, \lambda_1) = 1 - \left| \frac{r_{12} + r_{234} e^{2i\beta_2}}{1 + r_{12} r_{234} e^{2i\beta_2}} \right|^2$$

and

$$f_2(d_2, d_3, \lambda_2) = \frac{1}{1+a} \left| 1 + \sqrt{a} \frac{2\sqrt{N_1 N_2}}{N_1 + N_2} \frac{r_{234} e^{2i\beta_2}}{1 + r_{12} r_{234} e^{2i\beta_2}} \right|^2,$$

where, $r_{234} = \frac{r_{23} + r_{34} e^{2i\beta_3}}{1 + r_{23} r_{34} e^{2i\beta_3}}$, $r_{jk} = \frac{N_j \cos\theta_j - N_k \cos\theta_k}{N_j \cos\theta_j + N_k \cos\theta_k}$ (r_{jk} are the reflectance at interface of phase j and k), phase factor $\beta_j = 2\pi \left(\frac{d_j}{\lambda} \right) N_j$, d_j is the thickness of phase j, and θ_j is the incident or refractive angle of phase j and is zero at back-scattering configuration. "a" is defined as $a = I_{fore}/I_{back}$, where $I_{back} = \frac{1}{2} N_1 E_{10}^2$ and $I_{fore} = \frac{1}{2} N_2 E_{20}^2$ are the initial scattered or emitted intensity at the backward direction and forward direction, respectively. The

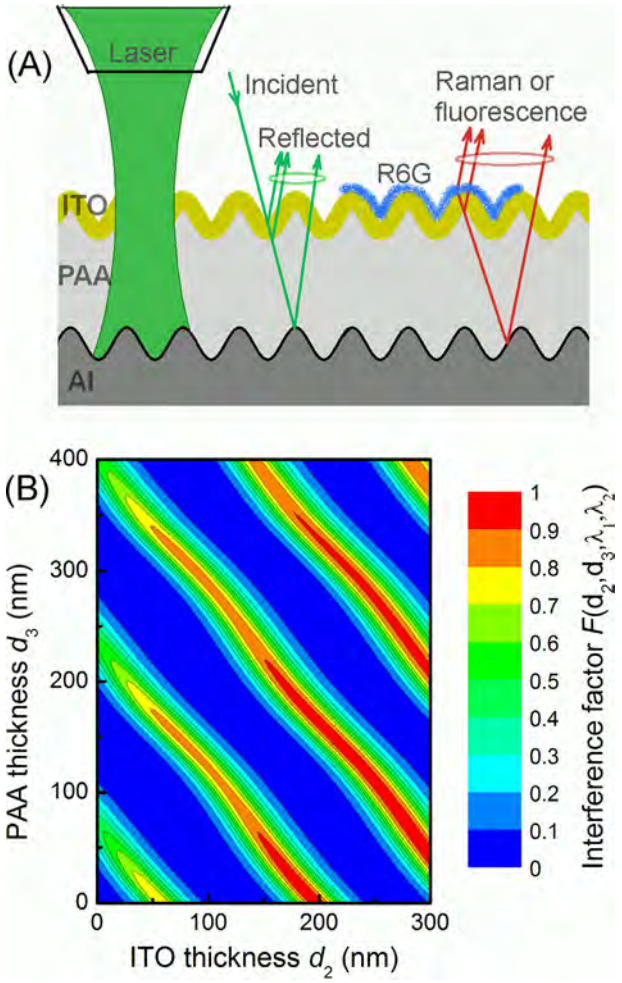

Fig. 5. (A) Schematic diagram of optical self-interference of the incident light and scattered light or emitted light. Multiple reflections happen within the transparent ITO layer and the PAA membrane. (B) Calculated interference factor map, as the function of the thicknesses of the PAA membrane and the ITO film. In calculations, parameters were set as $\lambda_1 = 514.5$ nm, $\lambda_2 = 531$ nm and $a = 3$.

complex refractive indexes are set as $N_1 = 1 + i0$, $N_2 = 1.886 + i0.032$ (514.5 nm) and $1.868 + i0.032$ (531 nm), $N_3 = n_{\text{eff}} + i0.003$, and $N_4 = 0.83 + i6.28$ [13,17,18]. The effective refractive index of the PAA membranes $n_{\text{eff}} = 1.586$–1.595 is obtained from the Bruggeman equation [19]: $(1-p)\frac{n_{\text{alumina}}^2 - n_{\text{eff}}^2}{n_{\text{alumina}}^2 + 2n_{\text{eff}}^2} + p\frac{1-n_{\text{eff}}^2}{1+2n_{\text{eff}}^2} = 0$, where n_{alumina} is 1.67 [20] and the porosity p of the PAA membranes is estimated to be 10.8–12.2% according to our microstructural observation (Table 1). Here, the thickness or thickness distribution of the porous ITO layers on the PAA membranes cannot be directly and precisely measured. Their mass-equal thicknesses obtained from the ITO layers on flat Si substrates are used in the calculation. Hence, we can use a refractive index n instead of an effective refractive index n_{eff} for the porous ITO layers in the calculation. The calculated Raman-intensity fluctuations with $F(d_2, d_3, \lambda_1, \lambda_2) = f_1(d_2, d_3, \lambda_1) \cdot f_2(d_2, d_3, \lambda_2)$ at $a = 3$ are shown in Fig. 4B–E and the calculated curves agree well with the experimental data with regard to the peak positions, which indicates that the above assumption on ITO film thickness is reasonable.

Fig. 5B shows the calculated interference factor 2D map as a function of the thickness of ITO film and PAA membrane. In this map, the regions with a high interference factor (red or yellow color) refer to the conditions under which a high Raman intensity is obtained. Such regions are sharp and long with a period of 138 nm (ITO thickness) and 165 nm (PAA thickness). This indicates that the thickness of both the ITO film and PAA membrane has to be controlled rigidly. Considering that the growth rate of the PAA membrane of 30–220 nm/min is quite large and fluctuations on the outer and inner surface, it is difficult to control precisely the thickness of the PAA membrane with a deviation of less than 10 nm. Here, ITO films with a limited thickness distribution are fabricated to compensate for the thickness deviation in the PAA membrane. The reflective interference fringes shown in Fig. S1 are useful in helping to identify rapidly the regions with a high interference factor. It should be noted that the detected intensity is the result of surface and interference co-enhancement. Figs. 4C–D shows that the left peak in the calculated curve is slightly weaker than the right peak, but the experimental results are opposite. The discrepancy between theoretical and experimental results arises from that the theoretical fitting only considers the modulation of optical interference on the Raman intensity whereas the Raman spectra are in fact co-enhanced by the interference and surface. In addition, a thin PAA membrane may help to decrease the fluorescence background, as shown in Fig. 3A. Therefore, besides the 2D map, a thinner ITO film and PAA membrane should be considered.

4. Summary

ITO nanocap arrays fabricated on PAA membranes are demonstrated to be excellent SERS substrates. A low detecting limit of R6G probes of 1×10^{-7} M or 50 ng/mL is achieved. Owing to the high transparency of both the ITO layer and PAA membrane, thin-film interferences strongly modulate the Raman spectra from molecules adsorbed on the ITO/PAA/Al substrate. The interference effect provides flexibility in sample preparation and can lead to surface and interference co-enhanced Raman scattering.

Acknowledgments

This work was jointly supported by the Natural Science Foundation of Jiangsu Province, China, under Grant No BK2012757, the National Natural Science Foundation of China under Grant Nos. 51271057 and 51071045, the Program for New Century Excellent Talents in University of Ministry of Eduction of China under Grant No. NCET-11-0096, the open research fund of Key Laboratory of MEMS of Ministry of Education, Southeast University, and Hong Kong Research Grants Council (RGC) Nos. CityU 112212 and 112510.

Appendix A. Supplementary data

Supplementary data associated with this article can be found, in the online version, at http://dx.doi.org/10.1016/j.apsusc.2013.04.158.

References

[1] C. Rhodes, S. Franzen, J.P. Maria, M. Losego, D.N. Leonard, B. Laughlin, G. Duscher, S. Weibel, Journal of Applied Physics 100 (2006) 054905.
[2] S. Szunerits, X. Castel, R. Boukherroub, Journal of Physical Chemistry C 112 (2008) 15813–15817.
[3] M. Kanehara, H. Koike, T. Yoshinaga, T. Teranishi, Journal of the American Chemical Society 131 (2009) 17736–17737.
[4] S. Franzen, Journal of Physical Chemistry C 112 (2008) 6027–6032.
[5] F. Michelotti, L. Dominici, E. Descrovi, N. Danz, F. Menchini, Optics Letters 34 (2009) 839–841.
[6] W.L. Barnes, A. Dereux, T.W. Ebbesen, Nature 424 (2003) 824–830.
[7] M. Fleischmann, P.J. Hendra, A.J. McQuillan, Chemical Physics Letters 26 (1974) 163–166.
[8] Y.M. Yang, T. Qiu, H.L. Ou, X.Z. Lang, Q.Y. Xu, F. Kong, W.J. Zhang, P.K. Chu, Journal of Physics D: Applied Physics 44 (2011) 215305.
[9] S.Q. Zhao, Y. Guo, S. Song, D. Choi, J.-i. Hahm, Applied Physics Letters 101 (2012) 053117.

[10] T. Qiu, W.J. Zhang, X.Z. Lang, Y.J. Zhou, T.J. Cui, P.K. Chu, Small 5 (2009) 2333–2337.
[11] X.Z. Lang, T. Qiu, W.J. Zhang, Y. Yin, P.K. Chu, Journal of Physical Chemistry C 115 (2011) 24328–24333.
[12] C.M. Galloway, P.G. Etchegoin, E.C. Le Ru, Physical Review Letters 103 (2009) 063003.
[13] Y.M. Yang, T. Qiu, F. Kong, J.Y. Fan, H.L. Ou, Q.Y. Xu, P.K. Chu, Journal of Applied Physics 111 (2012) 033110.
[14] D. Yoon, H. Moon, Y.W. Son, J.S. Choi, B.H. Park, Y.H. Cha, Y.D. Kim, H. Cheong, Physical Review B 80 (2009) 125422.
[15] K. Huang, L. Pu, Y. Shi, P. Han, R. Zhang, Y.D. Zheng, Applied Physics Letters 89 (2006) 201118.
[16] S. Gardelis, A.G. Nassiopoulou, V. Gianneta, M. Theodoropoulou, Journal of Applied Physics 107 (2010) 113104.
[17] J. Wang, C.W. Wang, Y. Li, W.M. Liu, Thin Solid Films 516 (2008) 7689–7694.
[18] C. Zhang, A.I. Smirnov, D. Hahn, H. Grebel, Chemical Physics Letters 440 (2007) 239–243.
[19] E.V. Astrova, V.A. Tolmachev, Materials Science and Engineering B 69 (2000) 142–148.
[20] J. Choi, Y. Luo, R.B. Wehrspohn, R. Hillebrand, J. Schilling, U. Gösele, Journal of Applied Physics 94 (2003) 4757–4762.